AMERICAN SOCIETY FOR MICROBIOLOGY | Journal of Virology®

VIRUS-CELL INTERACTIONS

Human Group C Rotavirus VP8*s Recognize Type A Histo-Blood Group Antigens as Ligands

Xiaoman Sun,[a,b] Lihong Wang,[c,a,b] Jianxun Qi,[d] Dandi Li,[a,b] Mengxuan Wang,[a,b] Xin Cong,[a,b] Ruchao Peng,[d] Wengang Chai,[e] Qing Zhang,[a,b] Hong Wang,[a,b] Hongling Wen,[c] George F. Gao,[b,d] Ming Tan,[f] Zhaojun Duan[a,b]

[a]Key Laboratory of Medical Virology and Viral Diseases, Ministry of Health of the People's Republic of China, Beijing, China

[b]National Institute for Viral Disease Control and Prevention, China CDC, Beijing, China

[c]Department of Virology, School of Public Health, Shandong University, Jinan, China

[d]CAS Key Laboratory of Pathogenic Microbiology and Immunology, Institute of Microbiology, Chinese Academy of Sciences, Beijing, China

[e]Glycosciences Laboratory, Department of Medicine, Imperial College London, London, United Kingdom

[f]Division of Infectious Diseases, University of Cincinnati College of Medicine, Cincinnati, Ohio, USA

ABSTRACT Group/species C rotaviruses (RVCs) have been identified as important pathogens of acute gastroenteritis (AGE) in children, family-based outbreaks, as well as animal infections. However, little is known regarding their host-specific interaction, infection, and pathogenesis. In this study, we performed serial studies to characterize the function and structural features of a human G4P[2] RVC VP8* that is responsible for the host receptor interaction. Glycan microarrays demonstrated that the human RVC VP8* recognizes type A histo-blood group antigens (HBGAs), which was confirmed by synthetic glycan-/saliva-based binding assays and hemagglutination of red blood cells, establishing a paradigm of RVC VP8*-glycan interactions. Furthermore, the high-resolution crystal structure of the human RVC VP8* was solved, showing a typical galectin-like structure consisting of two β-sheets but with significant differences from cogent proteins of group A rotaviruses (RVAs). The VP8* in complex with a type A trisaccharide displays a novel ligand binding site that consists of a particular set of amino acid residues of the C-D, G-H, and K-L loops. RVC VP8* interacts with type A HBGAs through a unique mechanism compared with that used by RVAs. Our findings shed light on the host-virus interaction and the coevolution of RVCs and will facilitate the development of specific antivirals and vaccines.

IMPORTANCE Group/species C rotaviruses (RVCs), members of *Reoviridae* family, infect both humans and animals, but our knowledge about the host factors that control host susceptibility and specificity is rudimentary. In this work, we characterized the glycan binding specificity and structural basis of a human RVC that recognizes type A HBGAs. We found that human RVC VP8*, the rotavirus host ligand binding domain that shares only ~15% homology with the VP8* domains of RVAs, recognizes type A HBGA at an as-yet-unknown glycan binding site through a mechanism distinct from that used by RVAs. Our new advancements provide insights into RVC-cell attachment, the critical step of virus infection, which will in turn help the development of control and prevention strategies against RVs.

KEYWORDS group/species C rotavirus (RVC), host factor, VP8* domain, crystal structure, type A HBGA, virus-glycan binding site

Rotaviruses (RVs), members of the *Rotavirus* genus in the family *Reoviridae*, are double-stranded RNA viruses causing acute gastroenteritis (AGE) in humans and animals (1). RVs are currently classified into nine groups/species (A to I) and a further

Received 15 March 2018 **Accepted** 16 March 2018

Accepted manuscript posted online 28 March 2018

Citation Sun X, Wang L, Qi J, Li D, Wang M, Cong X, Peng R, Chai W, Zhang Q, Wang H, Wen H, Gao GF, Tan M, Duan Z. 2018. Human group C rotavirus VP8*s recognize type A histo-blood group antigens as ligands. J Virol 92:e00442-18. https://doi.org/10.1128/JVI.00442-18.

Editor Susana López, Instituto de Biotecnologia/UNAM

Address correspondence to Zhaojun Duan, zhaojund@126.com.

X.S., L.W., J.Q., and D.L. contributed equally to this article.

tentative group J (2–4), among which group A, B, C, and H RVs infect both humans and animals, while groups D to G, I, and J cause diseases only in animal species. Group A RVs (RVAs) have been mostly studied and recognized as the leading cause of severe AGE worldwide (5). The RV genome consists of 11 double-stranded RNAs encoding 12 proteins, including 6 structural and 6 nonstructural proteins (1). RVs can be classified into different G and P genotypes on the basis of their outer capsid proteins, VP7 and VP4, respectively (6). The RV spike protein VP4 can be cleaved by trypsin into the VP5* and VP8* proteins, and the distally located VP8* domain is involved in interacting with host receptors to initiate an infection process (7–9).

RVAs have been shown to recognize cell surface glycans as ligands or receptors, which are crucial factors for viral attachment and entry. The available data indicate that various RVAs are able to bind variable glycans in a strain-specific manner (reviewed in references 10 and 11). For example, many animal RVAs tend to recognize the terminal sialic acids of sialoglycoconjugates, such as gangliosides, and some human RVAs can also interact with gangliosides with internal sialic acids (12, 13), while many other human RVAs interact with histo-blood group antigens (HBGAs), HBGA precursors, and/or mucins (13–23). These complex interactions between glycans and RVAs were shown to play an important role in RVA infections, host ranges, host tropisms, and cross-species transmission, highlighting the host-RV coevolution over time. However, the glycan binding features of other non-group A RVs remain rudimentary. Therefore, further study of the diverse RV-host glycan interactions would provide insights into RV epidemiology, prevalence, possible zoonotic transmission, and development of new prevention strategies against RVs.

Unlike RVAs, group/species C rotaviruses (RVCs) grow poorly in cell culture and have been studied only minimally. RVCs were reported to be associated with sporadic cases of diarrhea in children, family-based small outbreaks of gastroenteritis, and animal infections. RVCs causing diarrhea were first detected in pigs in 1980 (24) and were subsequently detected in bovines, dogs, and ferrets (25–27). They are now recognized as an important pathogen causing gastroenteritis in pigs in many countries. Surveillance studies showed that more than 70% of adult pigs exhibited RVC-reactive antibodies, indicating that RVCs circulate widely in pig populations (28). Sialic acids were reported to constitute an essential part of the cell receptor for the porcine group C virus (29). While the first human infection was reported in 1982 (30), RVCs are now known to be important pathogens causing diarrhea in humans of various age groups, including children and adults (31). A reported reassortment event of human RVCs in Hungary and the observation of both Indian-Bangladeshi and Far East Asian RVCs in Japan indicated that RVCs circulate widely (32–34). With implementation of the current RVA vaccines, RVA infections in humans have decreased worldwide (35–38), which may build up pressure prompting the emergence of new immune-escaping RVs (39, 40), and thus, it is of significance to document the circulation of other RVs, including RVCs.

The known RVCs have been sorted into 18 G and 21 P types (41). The reported human, bovine, and dog RVCs have been classified as G4P[2], G2P[3]/P[10], and G11P[11], respectively, while porcine RVCs show a similar diversity of 15 G and 17 P genotypes (41). The two outer capsid proteins (VP7 and VP4) are highly conserved among all human RVCs, sharing $>$95% sequence identity. Phylogenetic analysis based on VP7 and VP4 indicated that all human RVCs clustered tightly together, forming a single branch that, however, is distinct from other clusters of animal RVCs (42). In fact, our current understanding of RVCs, including their host ranges, epidemiology, evolution, interspecies transmission, and pathogenesis, remains limited. To this end, we set off to study the host factor interacting with the VP8* domain of human G4P[2] RVC and the interaction mechanism, aiming to advance our understanding of the virus-host interaction, host-specific infection, and evolution of RVCs.

RESULTS

VP8* glycan binding specificity of human RVCs. Our study started with the determination of the glycan binding specificity of human G4P[2] RVC VP8*, based on

the fact that the VP8* domain is responsible for host receptor interactions, which play a key role in specific host infection of RVs (reviewed in references 10 and 11). The recombinant VP8* proteins of two human RVC strains (Bristol and sz94) were produced as glutathione *S*-transferase (GST)-tagged proteins and were used as probes to perform glycan arrays against a glycan library containing 600 mammalian glycans (see Materials and Methods). Both VP8* proteins exhibited significant binding signals to more than a dozen glycans containing terminal sequences of GalNAcα1-3(Fucα1-2)Gal (Fuc, Gal, and GalNAc stand for fucose, galactose, and *N*-acetylgalactosamine, respectively), comprising the type A HBGAs (colored yellow in Fig. 1). In addition, the two GST-VP8* proteins also appeared to be binding signals to glycans containing a GlcNAcβ1-3Galβ1-4GlcNAc motif (glycan numbers 375, 538, and 548), although the binding signals of glycan 375 differed between the two proteins.

To further confirm the observed ligand binding specificity, we conducted glycan binding assays using synthetic oligosaccharides representing various HBGAs and sialic acids, including H type 1 (H1), H type 2 (H2), H type 3 (H3), type A and type B trisaccharides (A and B, respectively), Lewis a (Le^a), Lewis b (Le^b), Lewis x (Le^x), Lewis y (Le^y), type 1 and type 2 precursors (pre I and pre II, respectively), Neu5Ac, Neu5Gc, and sialyl-Le^x (sLe^x). The results showed that the VP8* proteins of human RVCs bound specifically to the oligosaccharides representing the type A HBGA (Fig. 2a). Furthermore, saliva-based binding assays showed that the VP8* proteins bound strongly to the type A and AB saliva samples (Fig. 2b), while the binding signals to the remaining saliva samples were significantly weaker. Finally, red blood cell (RBC) hemagglutination assays showed that the VP8* proteins were able to agglutinate type A and AB but not type O or B RBCs (Fig. 2c). Taken together, our data indicated clearly that the VP8* domains of human G4P[2] RVCs recognize type A HBGAs.

Structural features of the human RVC VP8*. To understand the structural basis of the observed binding feature between the human RVC VP8* and the type A HBGAs, the core VP8* domain (amino acids 64 to 224) of the Bristol strain was produced and crystallized. The high-resolution (1.8 Å) crystal structure of the core VP8* was solved (PDB accession number 5ZHG). Interestingly, human RVC VP8* exhibits a galectin-like folding typical of that of RVA VP8*s with two twisted antiparallel β-sheets that consist of strands C, D, G, H and A, L, B, I, J, K, respectively (Fig. 3a), although RVC VP8* shares only 15% sequence homology with the cognate proteins of RVAs. However, despite the similarity in their global folding, the RVC VP8* exhibits significant differences from RVA VP8*s, with the root mean square deviation (RMSD) value being more than 7 Å. First, RVC VP8* shows two longer β-strands, the βJ and βK strands, and the βL strand in RVA VP8* is replaced by a loop in the RVC VP8* (Fig. 3b). Second, RVC VP8* shows variations in the loop regions, including two longer loops, the J-K and C-D loops, and an alteration in the orientation of the G-H loop (Fig. 3b). Third, the region corresponding to the glycan binding site of the RVA VP8* is constituted by a completely new set of amino acids in the RVC VP8* (Fig. 3c and d). Fourth, unlike the positive electrostatic features in the RVA VP8*, the RVC VP8* reveals neutral and negative electrostatic properties (Fig. 3e and f; compare the boxes framed by dashed lines).

Identification of RVC glycan binding site. Identification of the RVC glycan binding site was achieved by solving the crystal structures of the RVC VP8* in complex with a type A trisaccharide. We cocrystallized the core VP8* proteins with synthetic type A trisaccharides [GalNAcα1-3(Fucα1-2)Gal] and obtained the crystal structures of the complex at high resolution (1.4 Å) (PDB accession number 5ZHO), showing clearly the density of the bound ligand (Fig. 4a). The type A trisaccharide binds to a cavity that consists of the C-D, G-H, and K-L loops (Fig. 4a). Compared with the native VP8* structure, no conformational changes caused by HBGA binding were noted. Both hydrogen bonds and hydrophobic interactions contribute to the HBGA binding (Fig. 4b to d). Both GalNAc and Fuc of the type A HBGA participate in the interactions. The GalNAc interacts with Ala110, Gly152, Arg206, and Ser207 through four hydrogen bonds, and the interaction was further stabilized by hydrophobic contacts with Leu109,

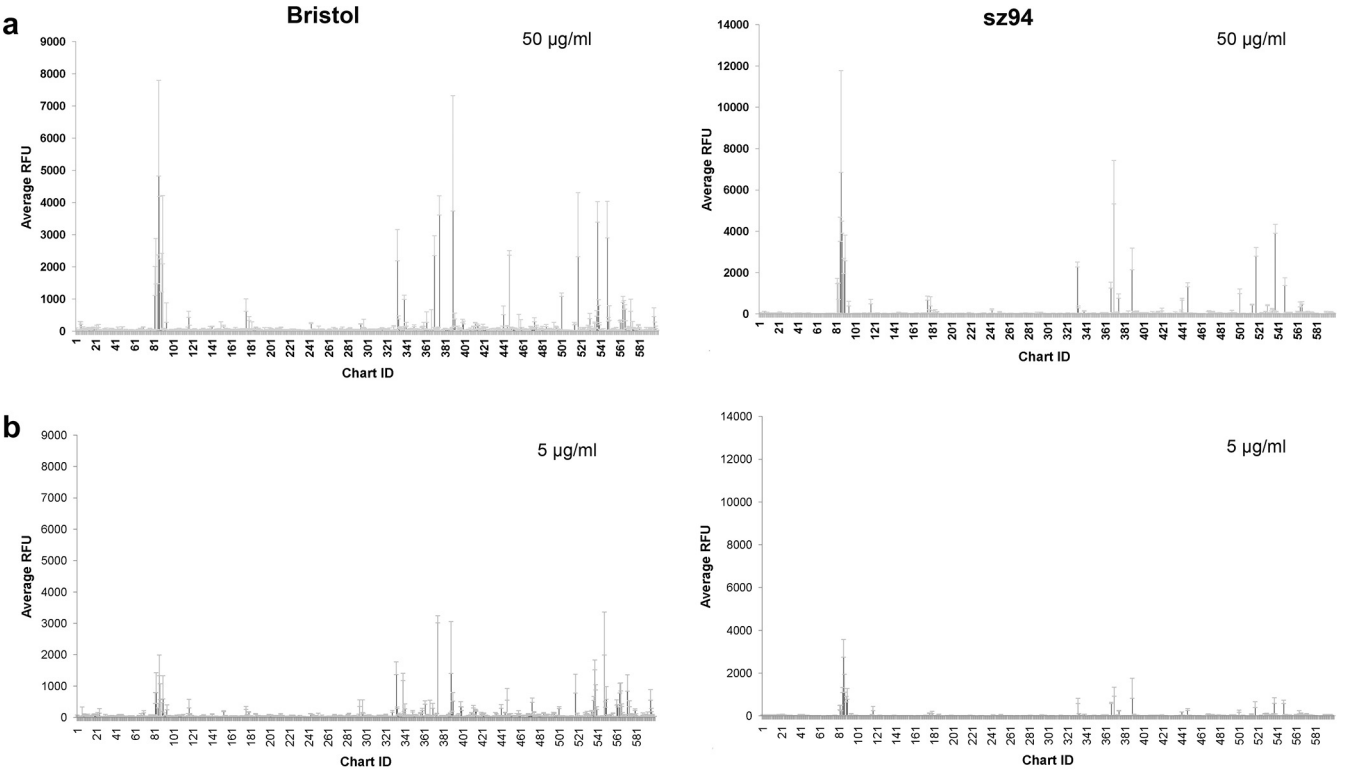

c

Chart ID	Glycan structure	50 μg/ml Average RFU	50 μg/ml StDev	50 μg/ml %CV	5 μg/ml Average RFU	5 μg/ml StDev	5 μg/ml %CV
86	GalNAca1-3(Fuca1-2)Galb1-4GlcNAcb-Sp8	6307	1483	24	1662	331	20
389	GalNAca1-3(Fuca1-2)Galb1-3GalNAca1-3(Fuca1-2)Galb1-4GlcNAcb-Sp0	5531	1792	32	2232	826	37
375	GalNAcb1-4GlcNAcb1-2Mana1-6(GalNAcb1-4GlcNAcb1-2Mana1-3)Manb1-4GlcNAcb1-4GlcNAc-Sp12	3910	295	8	3131	112	4
538	GlcNAcb1-3Galb1-4GlcNAcb1-3Galb1-4GlcNAcb1-2Mana1-6(GlcNAcb1-3Galb1-4GlcNAcb1-3Galb1-4GlcNAcb1-2Mana1-3)Manb1-4GlcNAcb1-4GlcNAcb-Sp25	3709	317	9	1677	156	9
548	GlcNAcb1-3Galb1-4GlcNAcb1-6(GlcNAcb1-3Galb1-4GlcNAcb1-2)Mana1-6(GlcNAcb1-3Galb1-4GlcNAcb1-2Man a1-3)Manb1-4GlcNAcb1-4GlcNAc-Sp24	3466	565	16	2680	682	25
518	GalNAca1-3(Fuca1-2)Galb1-4 GlcNAcb1-2Mana-Sp0	3307	995	30	1085	301	28
87	GalNAca1-3(Fuca1-2)Galb1-4Glcb-Sp0	3216	974	30	826	254	31
90	GalNAca1-3(Fuca1-2)Galb-Sp18	3157	1061	34	965	371	38
332	GalNAca1-3(Fuca1-2)Galb1-4GlcNAcb1-3Galb1-4GlcNAcb-Sp0	2675	486	18	1576	201	13
370	GalNAca1-3(Fuca1-2)Galb1-3GlcNAcb1-2Mana1-6(GalNAca1-3(Fuca1-2)Galb1-3GlcNAcb1-2Mana1-3)Manb1-4GlcNAcb1-4GlcNAcb-Sp20	2661	305	11	375	78	21
447	GalNAca1-3(Fuca1-2)Galb1-4GlcNAcb1-6(GalNAca1-3(Fuca1-2)Galb1-4GlcNAcb1-3)GalNAc-Sp14	2436	73	3	742	190	26
83	GalNAca1-3(Fuca1-2)Galb1-4(Fuca1-3)GlcNAcb-Sp0	2173	703	32	1109	317	29
85	GalNAca1-3(Fuca1-2)Galb1-4GlcNAcb-Sp0	1925	449	23	380	73	19
89	GalNAca1-3(Fuca1-2)Galb-Sp8	1819	604	33	336	137	41
82	GalNAca1-3(Fuca1-2)Galb1-3GlcNAcb-Sp0	1566	453	29	621	175	28
501	GalNAca1-3(Fuca1-2)Galb1-3GlcNAcb1-6GalNAca-Sp14	1133	52	5	316	29	9
Sp0= $CH_2CH_2NH_2$; Sp8=$CH_2CH_2CH_2NH_2$; Sp14= Threonine; Sp18=$O(CH_2)_2$ $NHCO(CH_2)5NH_2$; Sp20=GENR;							

Bristol

Chart ID	Glycan structure	50 μg/ml Average RFU	50 μg/ml StDev	50 μg/ml %CV	5 μg/ml Average RFU	5 μg/ml StDev	5 μg/ml %CV
86	GalNAca1-3(Fuca1-2)Galb1-4GlcNAcb-Sp8	9323	2463	26	3161	407	13
370	GalNAca1-3(Fuca1-2)Galb1-3GlcNAcb1-2Mana1-6(GalNAca1-3(Fuca1-2)Galb1-3GlcNAcb1-2Mana1-3)Manb1-4GlcNAcb1-4GlcNAcb-Sp20	6383	1045	16	1136	204	18
87	GalNAca1-3(Fuca1-2)Galb1-4Glcb-Sp0	4203	294	7	1529	420	27
538	GlcNAcb1-3Galb1-4GlcNAcb1-3Galb1-4GlcNAcb1-2Mana1-6(GlcNAcb1-3Galb1-4GlcNAcb1-3Galb1-4GlcNAcb1-2Mana1-3)Manb1-4GlcNAcb1-4GlcNAcb-Sp25	4128	222	5	721	126	18
85	GalNAca1-3(Fuca1-2)Galb1-4GlcNAcb-Sp0	4105	583	14	1218	113	9
90	GalNAca1-3(Fuca1-2)Galb-Sp18	3201	623	19	1035	251	24
518	GalNAca1-3(Fuca1-2)Galb1-4 GlcNAcb1-2Mana-Sp0	3013	208	7	522	137	26
389	GalNAca1-3(Fuca1-2)Galb1-3GalNAca1-3(Fuca1-2)Galb1-4GlcNAcb-Sp0	2664	519	19	1302	471	36
332	GalNAca1-3(Fuca1-2)Galb1-4GlcNAcb1-3Galb1-4GlcNAcb-Sp0	2393	121	5	701	117	17
89	GalNAca1-3(Fuca1-2)Galb-Sp8	2322	366	16	778	130	17
82	GalNAca1-3(Fuca1-2)Galb1-3GlcNAcb-Sp0	1593	124	8	386	102	26
548	GlcNAcb1-3Galb1-4GlcNAcb1-6(GlcNAcb1-3Galb1-4GlcNAcb1-2)Mana1-6(GlcNAcb1-3Galb1-4GlcNAcb1-2Man a1-3)Manb1-4GlcNAcb1-4GlcNAc-Sp24	1562	183	12	660	82	12
447	GalNAca1-3(Fuca1-2)Galb1-4GlcNAcb1-6(GalNAca1-3(Fuca1-2)Galb1-4GlcNAcb1-3)GalNAc-Sp14	1421	97	7	304	37	12
367	GalNAca1-3(Fuca1-2)Galb1-4GlcNAcb1-2Mana1-6(GalNAca1-3(Fuca1-2)Galb1-4GlcNAcb1-2Mana1-3)Manb1-4GlcNAcb1-4GlcNAcb-Sp20	1403	143	10	612	30	5
83	GalNAca1-3(Fuca1-2)Galb1-4(Fuca1-3)GlcNAcb-Sp0	1100	392	36	375	128	34
501	GalNAca1-3(Fuca1-2)Galb1-3GlcNAcb1-6GalNAca-Sp14	1100	112	10	225	47	21
Sp0= $CH_2CH_2NH_2$; Sp8=$CH_2CH_2CH_2NH_2$; Sp14= Threonine; Sp18=$O(CH_2)_2$ $NHCO(CH_2)5NH_2$; Sp20=GENR;							

sz94

FIG 1 Glycan binding specificity of two human RVC VP8*s (Bristol and sz94) determined through glycan arrays. (a and b) Graphical representation of binding of two GST-tagged human RVC (Bristol and sz94) VP8*s at 50 μg/ml (a) and 5 μg/ml (b) to 600 glycans in the array. Relative fluorescent units (RFU), corresponding to the strength of binding to individual glycans 1 to 600, are shown. (c) The top 16 glycans with the highest binding intensity, among which the ones containing the type A HBGA motif, GalNAcα1-3(Fucα1-2)Gal, are highlighted in yellow. The binding strengths at the two concentrations are shown. StDev, standard deviation; CV, coefficient of variation.

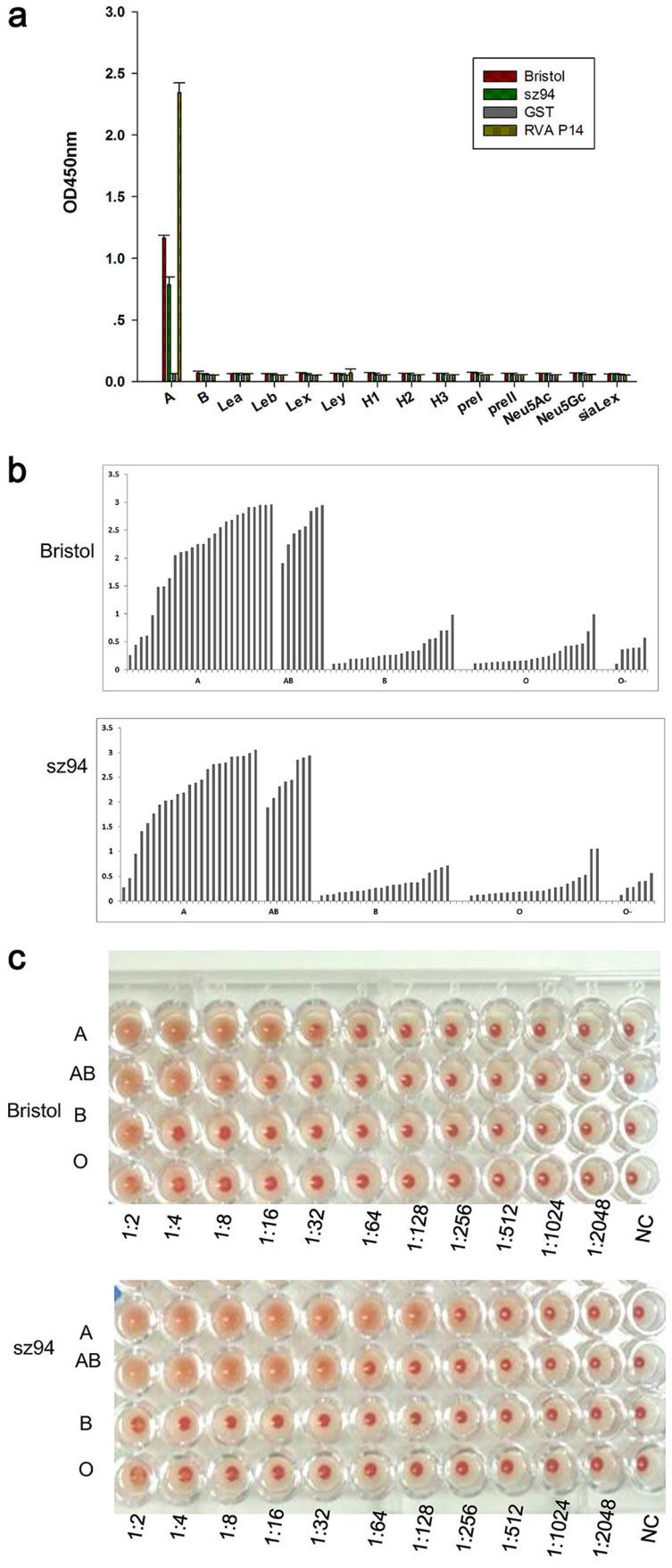
a
OD450nm
3.0
2.5
2.0
1.5
1.0
.5
0.0
Bristol
sz94
GST
RVA P14
A
B
Lea
Leb
Lex
Ley
H1
H2
H3
preI
preII
Neu5Ac
Neu5Gc
siaLex
b
Bristol
sz94
A
AB
B
O
O-
c
Bristol
sz94
A
AB
B
O
1:2
1:4
1:8
1:16
1:32
1:64
1:128
1:256
1:512
1:1024
1:2048
NC

Ala110, Glu151, Gly152, Pro205, and Ser207 (Fig. 4c and d). The Fuc forms two hydrogen-bonding interactions with Asn208 and two hydrophobic interactions involving Asn108 and Asn208. In contrast, the Gal of the type A trisaccharide projects out from the VP8* surface, showing no direct contact with the RVC VP8*.

The new binding mode and binding mechanism of human RVC. Compared to human P[14] RVA, which also recognizes type A HBGAs (15), the human P[2] RVC VP8* binds the same type A antigen through a distinct binding mode and mechanism. While the A antigen binding site of P[14] RVA VP8* is located within the cleft between the two β-sheets, the binding site of P[2] RVC VP8* moves away from the cleft. As a result, the RVC VP8* glycan binding site is a composed of nine residues (Asn108, Leu109, Ala110, Glu151, Gly152, Pro205, Arg206, Ser207, and Asn208) that showed no conservation with those of P[14] or other RVA glycan binding sites (Fig. 3d and 5a and b). Furthermore, the RVC binding site displays an electrostatically neutral feature at the bottom that accommodates the GalNAc and a negative edge region that interacts with the Fuc. These features are distinct from those of the RVA glycan binding sites, which are positive at the bottom region contacting GalNAc and negative at the region interacting with the Gal (Fig. 5c and d). In addition, the GalNAc and the Gal of the type A antigen participate in the interactions with the VP8* of P[14] RVA. In contrast, in the human RVC, the GalNAc (A epitope) interacts with six amino acids and thus plays the major role, and the Fuc (H epitope) interacts with two amino acids and thus plays a minor role, while the Gal is not involved in the interaction with the VP8* (Fig. 4d).

VP8* glycan binding specificity of animal RVCs. To further evaluate the glycan binding properties of animal RVCs, the VP8* proteins of two pig RVCs (porcine 1992 P[1], porcine 2011 P[5]), a dog RVC (dog 2012 P[11]), and a bovine RVC (bovine P[3]) were generated and used for binding assays. Saliva binding assays revealed that the VP8*s of the porcine 1992 P[1] and the dog 2012 P[11] RVCs preferably bound type A and type AB saliva samples (Fig. 6a), whereas porcine 2011 P[5] and bovine P[3] VP8*s did not bind any saliva samples. The VP8* of dog RVC (P[11]) hemagglutinated type A and type AB RBCs (Fig. 6b). These data suggest that some of the animal RVCs may share the ability to bind the type A HBGAs.

Genetic analyses of RVC VP8*s. A previous phylogenetic analysis based on 70 human, porcine, and bovine RVC VP4 genes revealed 9 P types (42), while another genome-wide genotyping analysis of RVCs from human, bovine, porcine, ferret, and canine sources showed 21 P genotypes (41). We focused here on the RVC VP8* protein sequences ($n = 72$), with our analysis indicating that human RVC VP8* proteins are highly conserved, and as a result, all VP8*s clustered tightly together, forming a single group (Fig. 7a). Bovine and dog RVC VP8* proteins clustered into another group containing three subgroups of P[3], P[10], and P[11] genotypes. Porcine RVC VP8*s were the most divergent, forming six major groups, each with various P genotypes (Fig. 7a).

Sequence alignments of the RVC VP8* proteins showed that all the nine amino acids involved in direct interactions with the type A HBGA were highly conserved among all human RVCs (data not shown), while one residue (residue 208) was changed in the VP8*s of bovine and dog RVCs. In porcine RVCs, variations were displayed in different groups. One, three, three, four, three, and two residues were changed in the first, second, third, fourth, fifth, and sixth groups, respectively (Fig. 7b).

FIG 2 Glycan binding specificity determination of human RVC VP8*s. (a) ELISA-based glycan binding assay. The binding signals (*y* axis) of the recombinant VP8* proteins at 20 μg/ml to synthetic oligosaccharides (2 μg/well) representing Lewis antigens (Le^a, Le^b, Le^x, and Le^y), A/B/H antigens (H1, H2, H3, A, B), the type 1 precursor (pre I), the type 2 precursor (pre II), and sialyl-Lex (sLe^x) (*x* axis) were determined. All oligosaccharides are conjugated with polyacrylamide (PAA) and biotin. The RVA P[14] GST-VP8* fusion protein and GST protein were included as a positive control and a negative control, respectively. OD450nm, optical density at 450 nm. (b) Saliva-based binding assay. The binding signals (*y* axis) of the human RVC GST-VP8* fusion proteins (20 μg/ml) to a panel of well-characterized saliva samples, including type A, AB, B, O, and nonsecretors (O−) (*x* axis), were determined. (c) Hemagglutination assay. Red blood cells of type A, AB, B, and O were mixed with various GST-VP8* proteins that were serially diluted with PBS, as indicated. PBS buffer without proteins was used as a negative control (NC).

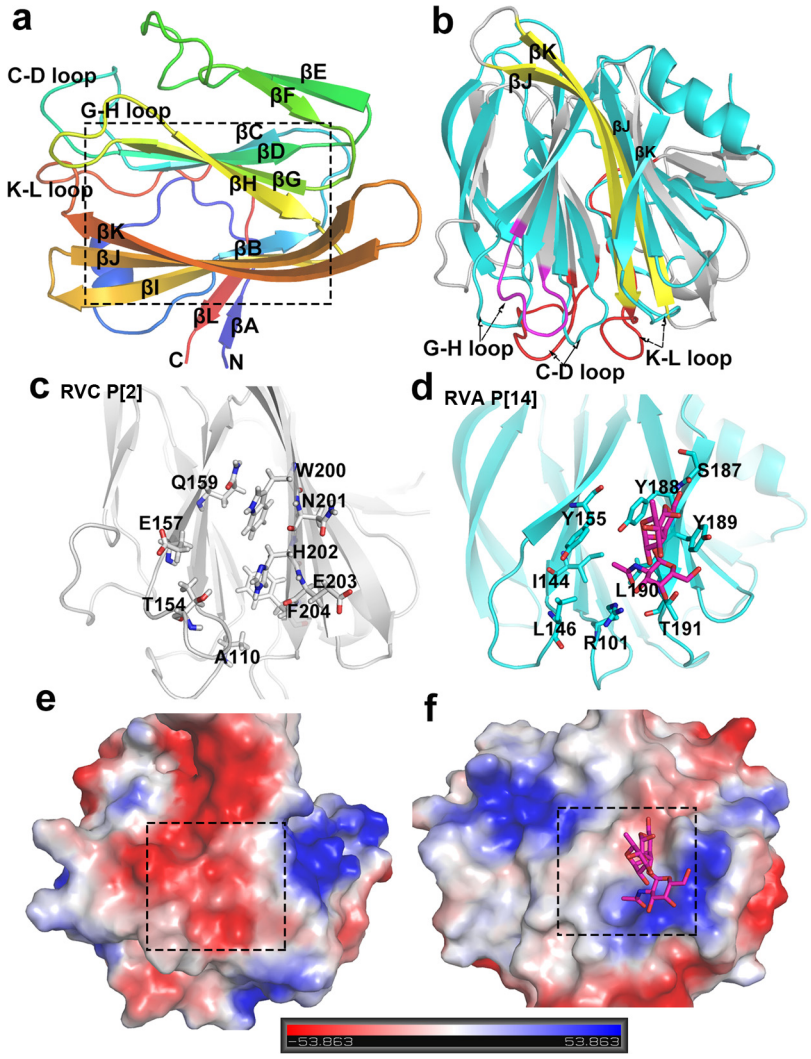

FIG 3 Crystal structure of the native human RVC VP8* and its comparison with that of the previously reported RVA P[14] VP8* (PDB accession number 4DRV). (a) Cartoon representation of the human RVC VP8* structure showing a galectin-like fold with two twisted β-sheets separated by a cleft (framed in the box). The N and C termini are denoted. (b) Structural alignment of the human RVC VP8* (gray) with the VP8* of human RVA P[14] RVA (cyan). The longer β-strands (βJ, βK), longer loops (C-D loop, K-L loop), and altered G-H loop in RVC VP8* are colored yellow, red, and magenta, respectively (arrows). (c and d) The glycan binding site in the human RVA P[14] VP8* (cyan) (d) and the corresponding site in the human RVC VP8* (gray) (c) (cartoon representation) with indications of the related amino acids (stick representation). (e and f) Comparison of the electrostatic surface potentials of the glycan binding sites between the human RVC VP8* (e) and the human RVA P[14] VP8* (f). Both VP8*s are shown in surface representation. The blue and red indicate the positive and negative electrostatic surface potentials, respectively. The glycan binding sites are framed by dashed-line boxes.

DISCUSSION

Previous studies have shown that the specific interactions between the RV VP8* domains and various glycans play an important role in viral infections, host tropisms, and interspecies transmissions of RVAs (11, 43, 44). To date, at least 10 different RV species have been identified (4), among which group A, B, and C RVs are the most common groups that infect both humans and animals. However, significant advances in understanding glycan-associated host ranges/host tropisms have been made only in RVAs, while little is known about other RV species. In this study, the VP8* structure, VP8*-glycan binding specificity, and structural basis of such VP8*-glycan interactions of an RVC were characterized. The finding that human RVC VP8* binds specifically to type A HBGA and the accurate delineation of the structural basis of such RVC VP8*-glycan

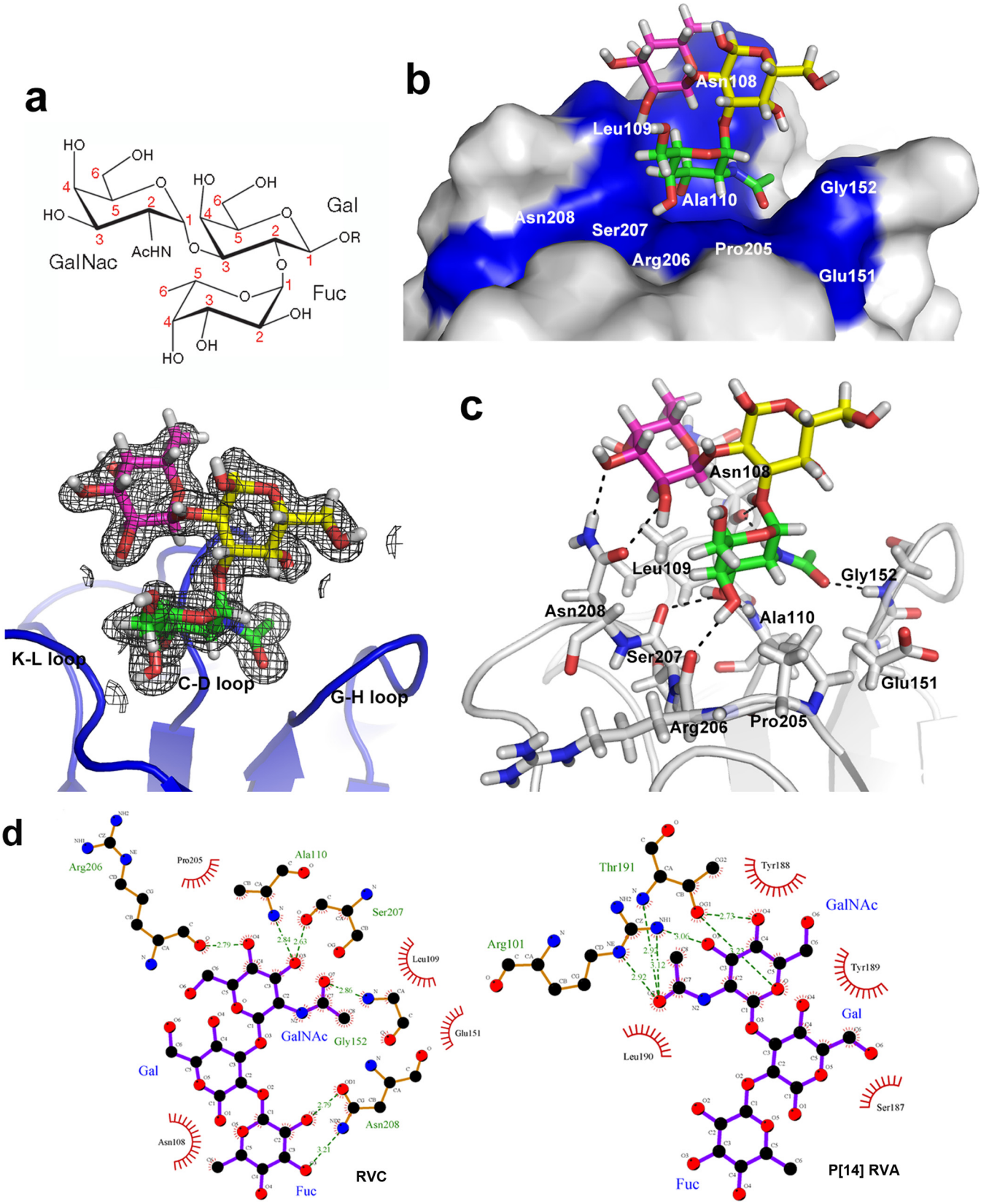

FIG 4 Structures of the glycan binding site of the human P[2] RVC VP8*. (a) Chemical structure of the type A trisaccharide (top) and the human RVC VP8* (bottom, blue) with an electron density map (mesh representation, gray) of the bound type A trisaccharide with calculated coefficients 2 $|F_o| - |F_c|$, contoured at the 1σ level (bottom). F_o and F_c are the observed and calculated structure factor amplitudes, respectively. The three sugars acetylgalactosamine (GalNAc), galactose (Gal), and fucose (Fuc) of the type A trisaccharide are shown in stick representation in green, yellow, and magenta, respectively, inside the map. The

(Continued on next page)

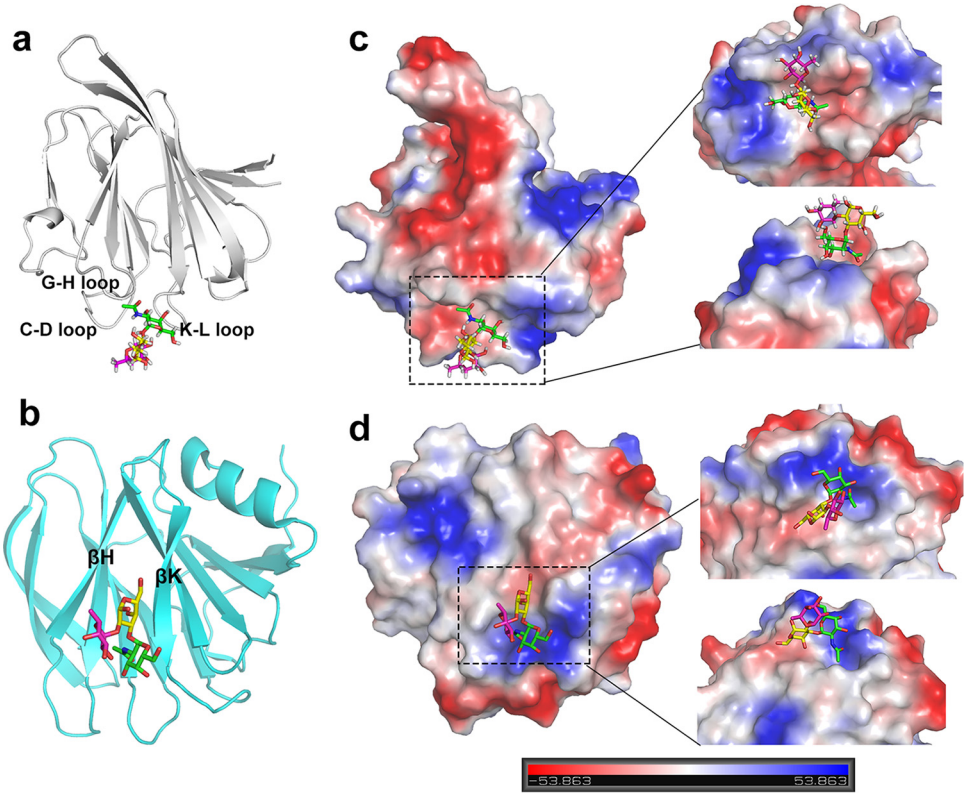

FIG 5 Human RVC VP8* binds the type A trisaccharide through a new glycan binding site via a binding mode and mechanism distinct from those for human P[14] RVA VP8* (PDB accession number 4DRV) reported previously. (a) The type A antigen (colored stick representation) binding site in the human RVC VP8* (cartoon representation, gray) is located outside the cleft between the two β-sheets. (b) The type A antigen (colored stick representation) binding site in the human P[14] RVA VP8* (cartoon representation, green) is located within the cleft between the two β-sheets. (c and d) The electrostatic surface potentials for the human RVC (c) and P[14] RVA (d) VP8*s (surface representations), with the type A antigen (colored stick representations) binding sites being indicated. Blue and red indicate the positive and negative charges, respectively. Panels c and d are in the same orientations as panels a and b. Detailed features of the type A antigen binding sites from the top view (top) and side view (bottom) are shown on the right.

interactions provide an important starting platform and approaches for future study of RVCs for better understanding of their evolution and epidemiology and for vaccine development.

In the present study, the VP8* proteins of two human RVC strains (Bristol and sz94) were demonstrated to recognize type A HBGAs. Phylogenetic analysis based on VP8* sequences showed that all human RVCs are clustered in a single P[2] genotype distinct from the animal RVCs (Fig. 7), suggesting a possibility that human RVCs may have evolved as a single lineage under the selection of the A antigens. In fact, human RVCs have been shown to circulate at a relatively low level worldwide and are associated with sporadic and limited outbreaks of gastroenteritis in both children and adult (31, 32). The observed binding of human RVC VP8* to only type A HBGAs and not B and H

FIG 4 Legend (Continued)
nitrogen and the oxygen atoms of the trisaccharide are colored in blue and red, respectively. The three loops (Fig. 3b) involved are labeled. (b) Surface representation of the P[2] RVC VP8* structure (gray) showing the bound type A trisaccharide in stick representation (with the same color scheme described in the legend to panel a). The acetamido group of GalNAc inserts into the binding pocket in the VP8* glycan binding site (blue). The amino acid residues that interact with the type A trisaccharide are indicated. (c) The hydrogen bonding network between the VP8* residues forming the glycan binding site (gray) and the type A trisaccharide is shown by dashed lines. (d) Detailed interactions between the human P[2] RVC Bristol VP8* and the type A trisaccharide ligand (left) compared with those of P[14] RVA HAL1166 (PDB accession number 4DRV) (right) determined using the LIGPLOT program. All the amino acid residues and the saccharide moiety involved in the interactions are labeled. The carbon, nitrogen, and oxygen atoms are represented by black, blue, and red circles, respectively. Hydrogen bond interactions are shown as green dashed lines, with the bond distances being indicated. The van der Walls contacts are indicated by an arc with spokes radiating toward the ligand atoms that they contact. The contacted atoms are shown with spokes radiating back.

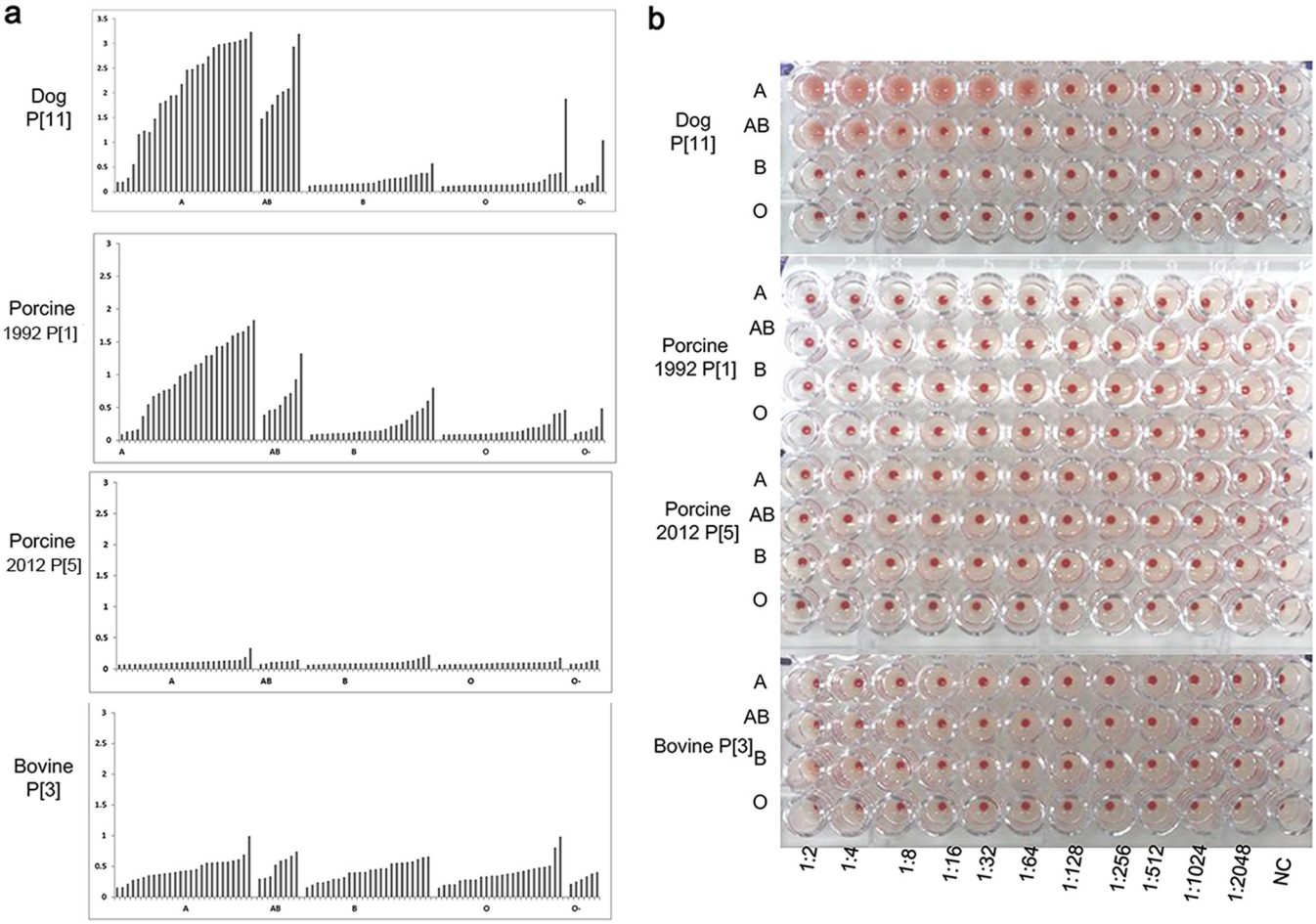

FIG 6 Determination of the glycan binding specificity of recombinant VP8* proteins of animal RVCs. (a) Recombinant VP8* proteins of four animal strains, including proteins from two pig RVCs (porcine 1992 P[1] and porcine 2011 P[5]), a dog RVC (dog 2012 P[11]), and a bovine RVC (bovine P[3]), at 20 μg/ml were applied to the test of binding to a panel of well-characterized saliva samples, including samples of type A, AB, B, and O and nonsecretors (O−) (*x* axis), in which the binding signals are shown on the *y* axis. (b) The hemagglutination activities of the animal RVC VP8*s were determined. Red blood cells of type A, AB, B, and O were mixed with various GST-VP8* proteins that were serially diluted with PBS, as indicated. PBS buffer without proteins was used as a negative control (NC).

antigens may partly restrain the RVC prevalence, as only a portion of the general population has the type A HBGA phenotype and other unknown virulence factors of RCVs may also contribute to the low prevalence of RCVs. Further studies to evaluate the association between the blood type A phenotype and the infection risk by human G4P[2] RVCs are required.

While retaining an overall galectin-like structure which is similar to that of RVA VP8*s (9), the human RVC VP8*s have gained distinct structural characteristics over the long course of evolution, including altered β-strand and loop regions. The narrower cleft resulting from the two longer β-strands and the alteration of the amino acid/surface features led to significant changes to the glycan binding site (Fig. 3), indicating a distinct ligand binding mechanism of RVCs. Furthermore, the changes of the C-D, G-H, and K-L loops result in the proximity of these loops, forming a cavity; all these structural changes contribute to the A antigen binding function of human RVC VP8*.

Like the reported P[14] RVA (15), the specific interactions between the type A antigen and the RVC VP8* strongly suggest that this type A HBGA may be a cell attachment factor for human RVCs. Sequence alignment indicated that all nine amino acids that constitute the glycan binding sites are highly conserved among human RVCs, implying that they are under tight functional and structural selection. Our data further suggest that human RVC VP8*s interact with type A antigen through a unique mech-

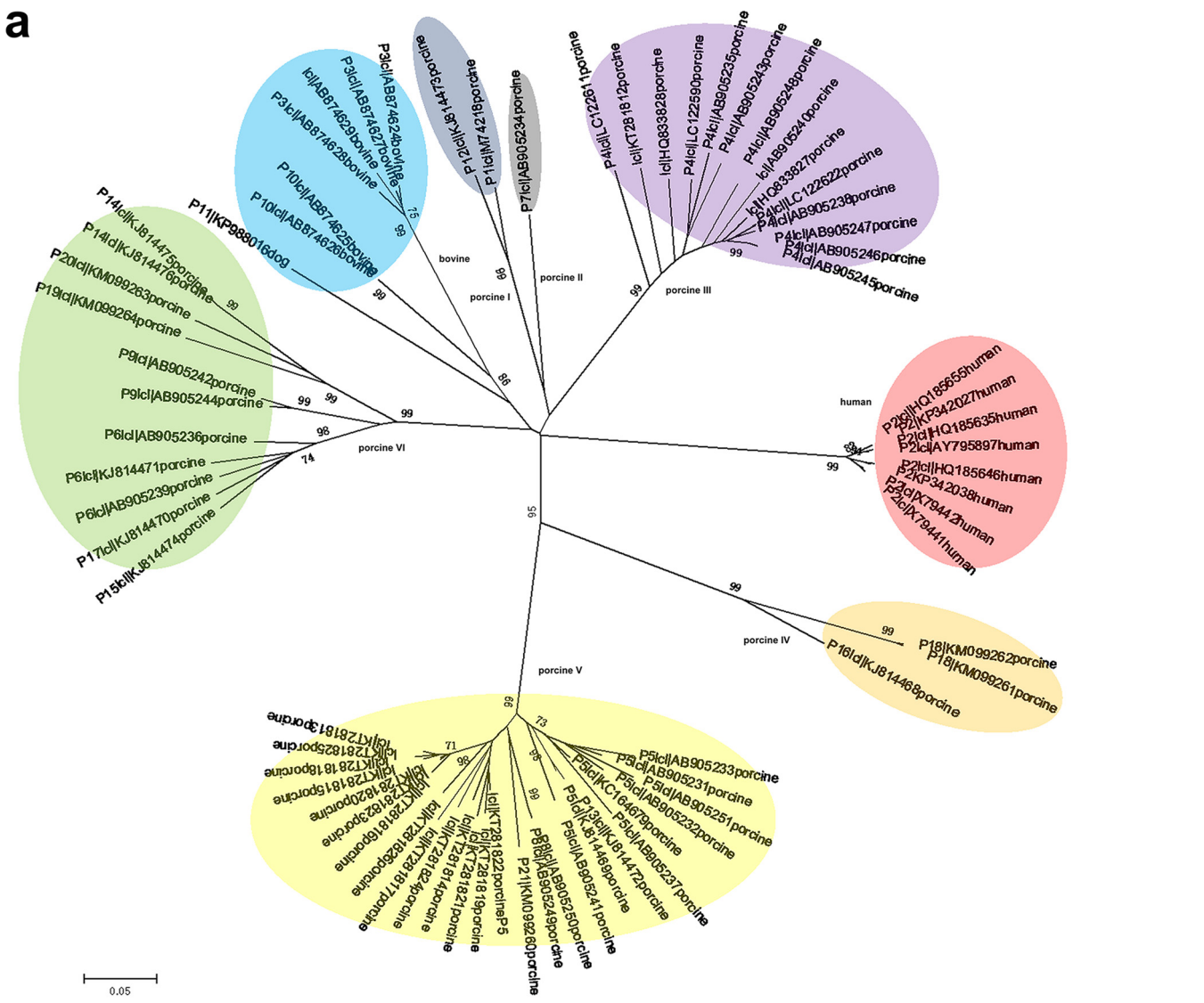

FIG 7 Phylogenetic analysis and sequence alignment of RVC VP8*s. (a) Evolutionary analyses were conducted using MEGA6 software, and the phylogenetic tree was constructed by the neighbor-joining method. The percentage of replicate trees in which the associated taxa clustered

(Continued on next page)

anism (Fig. 5) based on the following differences with RVA VP8*s: first, none of the nine amino acids that interact directly with the type A trisaccharide in VP8* of human RVCs is conserved with those of VP8* of RVAs; second, the binding site of human RVC VP8* is located at a different region with surface electrostatic features distinct from those of RVAs; and third, the VP8*s of RVCs and RVAs interact with different residues of the A trisaccharide. All these contribute to the different interaction mechanisms between VP8* and type A antigen, consistent with the fact that RVCs represent an evolutionary lineage distinct from RVAs.

RVCs have been found to infect both humans and animals. Type A HBGAs are also present in some animals, such as pigs, which exhibit high rates of infection by RVCs (28, 45). Although no cross-species transmission has been reported for RVCs, based on the limited surveillance conducted thus far, questions on such a possibility have been raised due to the shared host glycan factors. Our data showed variable binding characteristics for the bovine, dog, and porcine P[1] RVCs, though only one residue is different, suggesting that the specific amino acid residue 208 or other amino acids may affect the binding. Furthermore, some tested VP8*s of animal RVCs probably recognize A type HBGAs, including a porcine RVC (porcine 1992 P[1]) and a dog RVC (dog 2012 P[11]). These results suggest the possibility that some animal RVCs, especially the dog RVC (P[11]), the VP8* of which specifically hemagglutinated type A RBCs, may infect humans.

During our study, we also observed some phenomena that need further elucidation. We noted that the porcine 1992 P[1] VP8* that bound to A/AB-type saliva did not hemagglutinate type A or AB blood cells. This could be due to the weak binding function of animal RVC VP8*s to A-type HBGAs. Our previous experiments suggested that the enzyme-linked immunosorbent assay (ELISA) method is more sensitive for measurement of protein-glycan binding than the hemagglutination method. Thus, when such a binding function of a VP8* is weak, hemagglutination may not be a suitable method or at least not a sensitive method to detect such a weak binding signal. In addition, the two tested human RVC VP8*s also showed additional binding signals to glycans containing the GlcNAcβ1-3Galβ1-4GlcNAc motif, implying that glycans other than A antigen may also interact with the RVC VP8* as ligands. Meanwhile, the specificity and mechanism of such interaction still need further clarification, as it was also observed in a previous study of P[19] RV VP8* (17).

Two major RVA vaccines (Rotateq and Rotarix) have been widely used around the world and have helped to prevent gastroenteritis caused by RVAs (35–37, 46). Meanwhile, one cannot rule out the possibility that the use of these effective vaccines may lead to the emergence of new RVs (immune-escape mutants) that may cause RV epidemics. Therefore, more studies on the prevalence, infection, and pathogenesis of RVs, including RVCs, are necessary for their prevention and the development of control strategies. The virus-host interaction is an essential step in viral infection and also serves as an important target for vaccines and antivirals. Our findings of human RVC VP8* recognizing type A HBGA and the elucidation of the structural basis of this recognition open up a new avenue to explore the RVC-host interaction for new insights into RVC evolution and epidemiology and the development of vaccine approaches. The conserved glycan binding site among VP8*s of human RVCs revealed by this study may offer a target for future diagnostic/therapeutic antibodies and antivirals. Furthermore, enhanced surveillance of RVC infections in both humans and animals will fill the gaps in knowledge about the ecology of RVC in nature.

FIG 7 Legend (Continued)
together in the bootstrap test (1,000 replicates) is shown next to the branches. The tree was drawn to scale, with branch lengths being in the same units as those of the evolutionary distances used to infer the phylogenetic tree. The analysis involved 72 VP8* amino acid sequences (residues 1 to 231). Sequence information for the RVC strains is shown in the order of P genotype, GenBank accession number, and species. (b) Sequence alignment of RVC VP8* proteins of various P genotypes. Sequence alignment was done using the DNAMAN program. The residues involved in the glycan binding are labeled with numbers at the bottom. The conserved and varied residues are colored blue and green, respectively.

MATERIALS AND METHODS

Recombinant VP8* protein expression and purification. The cDNA fragments encoding VP8* domains (residues 1 to 231) of two human and four animal RVCs (human RVC Bristol [GenBank accession number X79442], human RVC sz94 [GenBank accession number KP342027], dog 2012 [GenBank accession number KP988016], porcine 1992 [GenBank accession number M74218], porcine 2011 [GenBank accession number KC164679], bovine [GenBank accession number AB738415]) were chemically synthesized by Genewiz Company (Suzhou, China) and individually cloned into the pGEX-4T-1 vector (GE Healthcare Life Sciences) with an N-terminal glutathione *S*-transferase (GST) tag. In addition, the DNA sequence encoding the VP8* core region (residues 64 to 224) of human RVC Bristol was cloned into the pET30a vector (Novagen) with a C-terminal hexahistidine (His×6) tag. The recombinant proteins were expressed in *Escherichia coli* strain BL21(DE3) induced with isopropyl-β-D-thiogalactopyranoside (IPTG) at a final concentration of 0.4 mM at 22°C for 16 h. The GST- and His-tagged proteins were purified as described previously (47). Briefly, the supernatant of bacterial lysates was filtered through a 0.22-μm-pore-size membrane (Millipore) and then loaded onto a glutathione-Sepharose (GE Healthcare Life Sciences) or HisTrap (GE Healthcare Life Sciences) column. The GST-fusion proteins were eluted with elution buffer (10 mM reduced glutathione, 50 mM Tris-HCl, pH 8.0) after washing five times with phosphate-buffered saline (PBS), which was changed to PBS buffer, and the proteins were concentrated using a 10-kDa concentration tube (Millipore) and centrifugation at 2,000 × *g* for about half an hour. The GST-VP8* fusion proteins were concentrated to about 20 mg/ml for further use. The His×6-tagged protein was eluted with PBS containing 300 mM imidazole following washing with PBS and PBS containing 20 mM imidazole. Purified proteins were analyzed by sodium dodecyl sulfate-polyacrylamide gel electrophoresis (SDS-PAGE). The VP8*-His×6 protein was further purified through a Superdex $200^{10/300GL}$ gel filtration column and concentrated with the 10-kDa concentration tube (Millipore) by centrifugation at a speed of 2,000 × *g* to about 20 mg/ml.

Glycan ligand screening of RVC VP8*s. Glycan ligand screening of RVC VP8*s was performed through the Protein-Glycan Interaction Resource under the Consortium for Functional Glycomics (CFG; http://www.functionalglycomics.org/) using our human RVC (Bristol, sz94) GST-VP8* fusion proteins as probes against a library containing 600 glycans. Two concentrations (5 μg/ml and 50 μg/ml) of each GST-VP8* protein were tested. A fluorescence-labeled anti-GST monoclonal antibody (Sigma) provided by the Protein-Glycan Interaction Resource was used as the detection antibody. Fluorescence was measured and quantified by a microarray scanner, and the relative fluorescent units (RFU) of each glycan were calculated (48).

Glycan binding assay. Enzyme-linked immunosorbent assay (ELISA)-based glycan binding assays were performed as described previously (16). The GST-VP8* fusion proteins at 0.2 mg/ml were coated onto microtiter plates at 100 μl per well. After incubation at 4°C overnight and blockage with 5% nonfat milk, synthetic oligosaccharides that were conjugated with polyacrylamide (PAA) and biotin were added at 2 μg per well. The oligosaccharides used in this study included Lewis a (Le^a), Lewis b (Le^b), Lewis x (Le^x), Lewis y (Le^y), H type 1 (H1), H type 2 (H2), H type 3 (H3), type A and type B trisaccharides (A and B, respectively), type 1 precursor (pre I), type 2 precursor (pre II), Neu5Ac, Neu5Gc, and sialyl-Le^x (sLe^x) (GlycoTech, Inc., Gaithersburg, MD). Then, horseradish peroxidase (HRP)-conjugated streptavidin (Abcam) was added at 0.1 μg per well. For each step, the plates were incubated at 37°C for 1 h, and between steps the plates were washed five times with 0.5% PBS-Tween 20 buffer. The color reactions were developed using a 3,3′,5,5′-tetramethylbenzidine (TMB) kit (BD Biosciences, San Diego), and the absorbance was measured at 450 nm.

Saliva binding assay. A panel of saliva samples with type ABO and secretor status (nonsecretors are labeled O negative [O−]) from Zhaojun Duan's lab stock was used for the saliva binding assays as previously described (16). Diluted saliva samples (1:1,000) were coated on microtiter plates at 4°C overnight. After blockage with 5% nonfat milk, GST-VP8* fusion proteins at 2 μg per well were added. After an incubation at 4°C overnight, mouse anti-GST antibody (Abcam) diluted at 1:3,000 was added at 100 μl per well, followed by adding horseradish peroxidase (HRP)-conjugated goat anti-mouse immunoglobulin antibody (1:10,000; Abgent). The color reactions were developed using the TMB kit, and the absorbance was measured at 450 nm. The plates were washed five times with 0.5% PBS-Tween 20 buffer between the above-mentioned steps.

Hemagglutination by GST-VP8* proteins. Human red blood cells (RBCs) of the A, AB, B, and O types (Immucor) were washed twice with PBS before use. The GST-VP8* proteins were 2-fold serially diluted starting at 2 mg/ml. The diluted proteins were added at 50 μl per well to 96-well V-bottom plates (Costar; Corning). A total of 50 μl of 1% RBCs was subsequently added. Agglutination was determined after 1 h of incubation at 25°C.

Evolutionary relationships of RVC VP8*. A phylogenetic tree was constructed with 72 VP8* protein sequences (amino acids 1 to 231), including those from 8 human RVCs, 1 dog RVC, 6 bovine RVCs, and 57 porcine RVCs. The evolutionary history was inferred using the neighbor-joining method. The percentage of replicate trees in which the associated taxa clustered together in the bootstrap test (1,000 replicates) is shown next to the branches. The evolutionary distances were computed using the Poisson correction method and are in units of the number of amino acid substitutions per site. Evolutionary analyses were conducted in MEGA6 software (49).

Protein crystallization. The His×6-tagged VP8* core protein was purified by gel filtration and buffered with 20 mM Tris-HCl, 50 mM NaCl, pH 8.0. The protein was concentrated to approximately 20 mg/ml, and crystallization screening was carried out using the sitting-drop vapor diffusion method at 18°C with 1 μl of protein mixed with 1 μl of reservoir solution. The native RVC Bristol VP8* was crystallized under the condition with 0.1 M sodium chloride, 0.1 M bis-Tris, pH 6.5, 1.5 M ammonium

TABLE 1 Crystallographic data collection and refinement statistics

Parameter[a]	Value(s) for[b]:		
	Native VP8*	VP8* soaked in NaI	VP8*-trisaccharide
Data collection statistics			
Space group	$P2_12_12_1$	$P2_12_12_1$	$P2_12_12_1$
Wavelength (Å)	1.5418	1.5418	0.9785
Unit cell dimensions			
a, *b*, *c* (Å)	38.07, 40.07, 124.01	38.08, 39.75, 123.70	37.99, 39.82, 119.81
α, β, γ (°)	90.00, 90.00, 90.00	90.00, 90.00, 90.00	90.00, 90.00, 90.00
Resolution (Å)	50.00–1.80 (1.86–1.80)	50.00–1.80 (1.86–1.80)	50.00–1.40 (1.45–1.40)
No. of observed reflections	188,451	194,134	463,155
Completeness (%)	99.4 (96.5)	96.7 (94.1)	99.0 (98.1)
Redundancy	10.3 (8.6)	11.0 (11.0)	11.3 (11.3)
R_{merge} (%)	9.9 (56.5)	11.5 (60.6)	9.6 (80.5)
$I/\sigma I$	21.0 (4.1)	24.8 (3.3)	28.6 (3.1)
Refinement statistics			
R_{work}/R_{free} (%)	17.98/20.40		14.13/17.38
No. of nonhydrogen atoms			
Protein	1334		1365
Ligands	0		36
Water	208		204
B factors			
Protein	21.8		19.3
Ligands			23.4
Water	35.4		30.4
RMSD			
Bond lengths (Å)	0.004		0.008
Bond angles (°)	0.697		0.828
Ramachandran plot (%)			
Favored	97.5		96.9
Allowed	1.88		3.1
Outliers	0.62		0.0

[a]$R_{merge} = \Sigma hkl\ |I - <I>|/\Sigma hkl I$, where *I* is the intensity of unique reflection hkl and $<I>$ is the average for symmetry-related observations of unique reflection hkl. Vectors and planes in a crystal lattice are described by the three-value Miller index notation. This syntax uses the indices h, k, and l as directional orthogonal parameters, which are separated by 90°. Each reflection is located by its three-dimensional coordinates h, k, and l.
[b]Values in parentheses are for the highest-resolution shell.

sulfate. The native VP8* crystal was also soaked with sodium iodide in order to solve the structure. Sodium iodide (Sigma) was dissolved in double-distilled H_2O (ddH_2O) at a concentration of 5 M, and the VP8* crystal was incubated with sodium iodide at a final concentration of 1.2 M for 1 min before the X-ray diffraction studies. For cocrystallization, type A trisaccharide was dissolved in ddH_2O at 100 mM. The VP8* protein was cocrystallized with the type A trisaccharide at a molar ratio of 1:50. VP8*-A complex crystals grow under the same conditions as the native protein.

Data collection and processing. The native and the derivative X-ray diffraction data were collected at an in-house X-ray facility, while the data for the complex were collected at Shanghai Synchrotron Radiation Facility (SSRF) beamline 19U. All data were processed with HKL2000 software (50). Additional processing was performed with programs from the CCP4 suite (51). The structure of VP8* was determined by the single-wavelength anomalous diffraction (SAD) method. The iodine sites were first located by SHELXD (52) for the I-SAD data. The identified positions were then refined, and the phases were calculated with the SAD experimental phasing module of PHASER (53). The real space constraints were further applied to the electron density map in density modification (DM) (54). The initial model was built with Autobuild in the PHENIX package (53). Additional missing residues were added manually in the COOT program (55). The model was further refined with phenix.refine (56) in the PHENIX package (57) with energy minimization, ADP refinement, and bulk solvent modeling. The native VP8* and the complex VP8*-trisaccharide structures were then solved by the molecular replacement module of PHASER (53), with the derivative VP8* structure being used as the search models. The stereochemical quality of the final model was assessed with the MolProbity program (58). Data collection and refinement statistics are summarized in Table 1. The structural analysis was done with the PyMOL program (http://www.pymol.org/pymol). The root mean square deviation (RMSD) is the measure of the average distance between the backbone atoms of superimposed proteins. The RMSD value was calculated using the align function in PyMOL.

Accession number(s). The crystal structure of the core VP8* of RCV has been submitted to the Protein Data Bank (PDB) and may be found under accession number 5ZHG. The crystal structure of core VP8* proteins cocrystallized with synthetic type A trisaccharides [GalNAcα1-3(Fucα1-2)Gal] has also been submitted to PDB and may be found under accession number 5ZHO.

ACKNOWLEDGMENTS

We thank Yi Shi and Jinghua Yan of the Institute of Microbiology, Chinese Academy of Sciences, for their suggestions on the manuscript. We thank Lili Li, Yuanyun Ao, Miao Jin, Xiangyu Kong, Lili Pang, Yue Yuan, and Huiying Li at the National Institute for Viral Disease Control and Prevention for their help with the performance of the experiments and data analysis. We thank Shuijun Zhang of the Duke-National University of Singapore Medical School for advice on structural data analysis. We also thank Yuan Yuan, Min Zhao, Yan Li, Xu Yang, and Yingzi Cui of the Institute of Microbiology for their help with crystal production and X-ray data collection. We thank Jingyu Yan of the Dalian Institute of Chemical Physics for her help with the analysis of the glycans. We acknowledge Yi Han of the Institute of Biophysics for help with X-ray data collection. The assistance provided by the staff at the Shanghai Synchrotron Radiation Facility (SSRF; beamline 19U) is acknowledged.

We all declare no potential conflicts of interest.

Zhaojun Duan, Xiaoman Sun, and Dandi Li designed the experiments. Lihong Wang, Xiaoman Sun, Dandi Li, Mengxuan Wang, and Xin Cong conducted the experiments. Jianxun Qi and Ruchao Peng collected the X-ray data. Jianxun Qi solved the structures. Xiaoman Sun, Dandi Li, Wengang Chai, Qing Zhang, Hong Wang, Hongling Wen, and Ming Tan analyzed the glycan binding data. Xiaoman Sun, Jianxun Qi, Ruchao Peng, and George F. Gao interpreted the structural data. Xiaoman Sun wrote the draft manuscript. George F. Gao, Ming Tan, and Zhaojun Duan revised the manuscript.

We acknowledge the participation of the Protein-Glycan Interaction Resource of CFG (supporting grant R24 GM098791) and the National Center for Functional Glycomics (NCFG) at Beth Israel Deaconess Medical Center, Harvard Medical School (supporting grant P41 GM103694), in the analysis of samples by use of a glycan microarray. This research was supported by grants from the National Key R&D program of China (Special National Project on Research and Development of Key Biosafety Technologies [2016YFC1201900]) and the National Natural Science Foundation of China (NSFC) (no. 81472003, no. 31500139, and no. 81601813).

REFERENCES

1. Estes MK, Greenberg HB. 2013. Rotaviruses, p 1347–1401. *In* Knipe DM, Howley PM, Cohen JI, Griffin DE, Lamb RA, Martin MA, Racaniello VR, Roizman B (ed), Fields virology, 6th ed. Lippincott Williams & Wilkins, Philadelphia, PA.
2. Matthijnssens J, Otto PH, Ciarlet M, Desselberger U, Van Ranst M, Johne R. 2012. VP6-sequence-based cutoff values as a criterion for rotavirus species demarcation. Arch Virol 157:1177–1182. https://doi.org/10.1007/s00705-012-1273-3.
3. Mihalov-Kovács E, Gellért Á Marton S, Farkas SL, Fehér E, Oldal M, Jakab F, Martella V, Bányai K. 2015. Candidate new rotavirus species in sheltered dogs, Hungary. Emerg Infect Dis 21:660–663. https://doi.org/10.3201/eid2104.141370.
4. Banyai K, Kemenesi G, Budinski I, Foldes F, Zana B, Marton S, Varga-Kugler R, Oldal M, Kurucz K, Jakab F. 2017. Candidate new rotavirus species in Schreiber's bats, Serbia. Infect Genet Evol 48:19–26. https://doi.org/10.1016/j.meegid.2016.12.002.
5. Tate JE, Burton AH, Boschi-Pinto C, Steele AD, Duque J, Parashar UD, WHO-Coordinated Global Rotavirus Surveillance Network. 2012. 2008 estimate of worldwide rotavirus-associated mortality in children younger than 5 years before the introduction of universal rotavirus vaccination programmes: a systematic review and meta-analysis. Lancet Infect Dis 12:136–141. https://doi.org/10.1016/S1473-3099(11)70253-5.
6. Matthijnssens J, Ciarlet M, McDonald SM, Attoui H, Banyai K, Brister JR, Buesa J, Esona MD, Estes MK, Gentsch JR, Iturriza-Gomara M, Johne R, Kirkwood CD, Martella V, Mertens PP, Nakagomi O, Parreno V, Rahman M, Ruggeri FM, Saif LJ, Santos N, Steyer A, Taniguchi K, Patton JT, Desselberger U, Van Ranst M. 2011. Uniformity of rotavirus strain nomenclature proposed by the Rotavirus Classification Working Group (RCWG). Arch Virol 156:1397–1413. https://doi.org/10.1007/s00705-011-1006-z.
7. Padilla-Noriega L, Dunn SJ, Lopez S, Greenberg HB, Arias CF. 1995. Identification of two independent neutralization domains on the VP4 trypsin cleavage products VP5* and VP8* of human rotavirus ST3. Virology 206:148–154. https://doi.org/10.1016/S0042-6822(95)80029-8.
8. Fiore L, Greenberg HB, Mackow ER. 1991. The VP8 fragment of VP4 is the rhesus rotavirus hemagglutinin. Virology 181:553–563. https://doi.org/10.1016/0042-6822(91)90888-I.
9. Dormitzer PR, Sun ZY, Wagner G, Harrison SC. 2002. The rhesus rotavirus VP4 sialic acid binding domain has a galectin fold with a novel carbohydrate binding site. EMBO J 21:885–897. https://doi.org/10.1093/emboj/21.5.885.
10. Tan M, Jiang X. 2014. Histo-blood group antigens: a common niche for norovirus and rotavirus. Expert Rev Mol Med 16:e5. https://doi.org/10.1017/erm.2014.2.
11. Jiang X, Liu Y, Tan M. 2017. Histo-blood group antigens as receptors for rotavirus, new understanding on rotavirus epidemiology and vaccine strategy. Emerg Microbes Infect 6:e22. https://doi.org/10.1038/emi.2017.30.
12. Fleming FE, Bohm R, Dang VT, Holloway G, Haselhorst T, Madge PD, Deveryshetty J, Yu X, Blanchard H, von Itzstein M, Coulson BS. 2014. Relative roles of GM1 ganglioside, N-acylneuraminic acids, and alpha2beta1 integrin in mediating rotavirus infection. J Virol 88:4558–4571. https://doi.org/10.1128/JVI.03431-13.
13. Haselhorst T, Fleming FE, Dyason JC, Hartnell RD, Yu X, Holloway G, Santegoets K, Kiefel MJ, Blanchard H, Coulson BS, von Itzstein M. 2009. Sialic acid dependence in rotavirus host cell invasion. Nat Chem Biol 5:91–93. https://doi.org/10.1038/nchembio.134.
14. Isa P, Arias CF, Lopez S. 2006. Role of sialic acids in rotavirus infection. Glycoconj J 23:27–37. https://doi.org/10.1007/s10719-006-5435-y.
15. Hu L, Crawford SE, Czako R, Cortes-Penfield NW, Smith DF, Le Pendu J, Estes MK, Prasad BV. 2012. Cell attachment protein VP8* of a human rotavirus specifically interacts with A-type histo-blood group antigen. Nature 485:256–259. https://doi.org/10.1038/nature10996.

16. Huang P, Xia M, Tan M, Zhong W, Wei C, Wang L, Morrow A, Jiang X. 2012. Spike protein VP8* of human rotavirus recognizes histo-blood group antigens in a type-specific manner. J Virol 86:4833–4843. https://doi.org/10.1128/JVI.05507-11.
17. Liu Y, Ramelot TA, Huang P, Liu Y, Li Z, Feizi T, Zhong W, Wu FT, Tan M, Kennedy MA, Jiang X. 2016. Glycan specificity of P[19] rotavirus and comparison with those of related P genotypes. J Virol 90:9983–9996. https://doi.org/10.1128/JVI.01494-16.
18. Ma X, Li DD, Sun XM, Guo YQ, Xiang JY, Wang WH, Zhang LX, Gu QJ, Duan ZJ. 2015. Binding patterns of rotavirus genotypes P[4], P[6], and P[8] in China with histo-blood group antigens. PLoS One 10:e0134584. https://doi.org/10.1371/journal.pone.0134584.
19. Hu L, Ramani S, Czako R, Sankaran B, Yu Y, Smith DF, Cummings RD, Estes MK, Venkataram Prasad BV. 2015. Structural basis of glycan specificity in neonate-specific bovine-human reassortant rotavirus. Nat Commun 6:8346. https://doi.org/10.1038/ncomms9346.
20. Liu Y, Xu S, Woodruff AL, Xia M, Tan M, Kennedy MA, Jiang X. 2017. Structural basis of glycan specificity of P[19] VP8*: implications for rotavirus zoonosis and evolution. PLoS Pathog 13:e1006707. https://doi.org/10.1371/journal.ppat.1006707.
21. Kazi AM, Cortese MM, Yu Y, Lopman B, Morrow AL, Fleming JA, McNeal MM, Steele AD, Parashar UD, Zaidi AKM, Ali A. 2017. Secretor and salivary ABO blood group antigen status predict rotavirus vaccine take in infants. J Infect Dis 215:786–789. https://doi.org/10.1093/infdis/jix028.
22. Sun X, Guo N, Li D, Jin M, Zhou Y, Xie G, Pang L, Zhang Q, Cao Y, Duan ZJ. 2016. Binding specificity of P[8] VP8* proteins of rotavirus vaccine strains with histo-blood group antigens. Virology 495:129–135. https://doi.org/10.1016/j.virol.2016.05.010.
23. Bohm R, Fleming FE, Maggioni A, Dang VT, Holloway G, Coulson BS, von Itzstein M, Haselhorst T. 2015. Revisiting the role of histo-blood group antigens in rotavirus host-cell invasion. Nat Commun 6:5907. https://doi.org/10.1038/ncomms6907.
24. Saif LJ, Bohl EH, Theil KW, Cross RF, House JA. 1980. Rotavirus-like, calicivirus-like, and 23-nm virus-like particles associated with diarrhea in young pigs. J Clin Microbiol 12:105–111.
25. Mawatari T, Taneichi A, Kawagoe T, Hosokawa M, Togashi K, Tsunemitsu H. 2004. Detection of a bovine group C rotavirus from adult cows with diarrhea and reduced milk production. J Vet Med Sci 66:887–890. https://doi.org/10.1292/jvms.66.887.
26. Park SI, Jeong YJ, Kim HJ, Park JG, Kang SY, Woo SK, Kim CH, Jung CH, Kang MI, Cho KO. 2011. Genetically diverse group C rotaviruses cause sporadic infection in Korean calves. J Vet Med Sci 73:479–482. https://doi.org/10.1292/jvms.10-0280.
27. Marton S, Mihalov-Kovacs E, Doro R, Csata T, Feher E, Oldal M, Jakab F, Matthijnssens J, Martella V, Banyai K. 2015. Canine rotavirus C strain detected in Hungary shows marked genotype diversity. J Gen Virol 96:3059–3071. https://doi.org/10.1099/jgv.0.000237.
28. Vlasova A, Amimo J, Saif L. 2017. Porcine rotaviruses: epidemiology, immune responses and control strategies. Viruses 9:48. https://doi.org/10.3390/v9030048.
29. Svensson L. 1992. Group C rotavirus requires sialic acid for erythrocyte and cell receptor binding. J Virol 66:5582–5585.
30. Bohl EH, Saif LJ, Theil KW, Agnes AG, Cross RF. 1982. Porcine pararotavirus: detection, differentiation from rotavirus, and pathogenesis in gnotobiotic pigs. J Clin Microbiol 15:312–319.
31. Nilsson M, Svenungsson B, Hedlund KO, Uhnoo I, Lagergren A, Akre T, Svensson L. 2000. Incidence and genetic diversity of group C rotavirus among adults. J Infect Dis 182:678–684. https://doi.org/10.1086/315772.
32. Kumazaki M, Usuku S. 2014. Epidemiological and genetic analysis of human group C rotaviruses isolated from outbreaks of acute gastroenteritis in Yokohama, Japan, between 2006 and 2012. Arch Virol 159:761–771. https://doi.org/10.1007/s00705-013-1894-1.
33. Doan YH, Haga K, Fujimoto A, Fujii Y, Takai-Todaka R, Oka T, Kimura H, Yoshizumi S, Shigemoto N, Okamoto-Nakagawa R, Shirabe K, Shinomiya H, Sakon N, Katayama K. 2016. Genetic analysis of human rotavirus C: the appearance of Indian-Bangladeshi strain in Far East Asian countries. Infect Genet Evol 41:160–173. https://doi.org/10.1016/j.meegid.2016.03.027.
34. Marton S, Deak J, Doro R, Csata T, Farkas SL, Martella V, Banyai K. 2015. Reassortant human group C rotaviruses in Hungary. Infect Genet Evol 34:410–414. https://doi.org/10.1016/j.meegid.2015.05.007.
35. Cortes JE, Curns AT, Tate JE, Cortese MM, Patel MM, Zhou F, Parashar UD. 2011. Rotavirus vaccine and health care utilization for diarrhea in U.S. children. N Engl J Med 365:1108–1117. https://doi.org/10.1056/NEJMoa1000446.
36. Dennehy PH. 2012. Effects of vaccine on rotavirus disease in the pediatric population. Curr Opin Pediatr 24:76–84. https://doi.org/10.1097/MOP.0b013e32834ee594.
37. Leshem E, Moritz RE, Curns AT, Zhou F, Tate JE, Lopman BA, Parashar UD. 2014. Rotavirus vaccines and health care utilization for diarrhea in the United States (2007–2011). Pediatrics 134:15–23. https://doi.org/10.1542/peds.2013-3849.
38. Pecenka C, Parashar U, Tate JE, Khan JAM, Groman D, Chacko S, Shamsuzzaman M, Clark A, Atherly D. 2017. Impact and cost-effectiveness of rotavirus vaccination in Bangladesh. Vaccine 35:3982–3987. https://doi.org/10.1016/j.vaccine.2017.05.087.
39. Pitzer VE, Bilcke J, Heylen E, Crawford FW, Callens M, De Smet F, Van Ranst M, Zeller M, Matthijnssens J. 2015. Did large-scale vaccination drive changes in the circulating rotavirus population in Belgium? Sci Rep 5:18585. https://doi.org/10.1038/srep18585.
40. Jere KC, Chaguza C, Bar-Zeev N, Lowe J, Peno C, Kumwenda B, Nakagomi O, Tate JE, Parashar UD, Heyderman RS, French N, Cunliffe NA, Iturriza-Gomara M. 2018. Emergence of double- and triple-gene reassortant G1P[8] rotaviruses possessing a DS-1-like backbone after rotavirus vaccine introduction in Malawi. J Virol 92:e01246-17. https://doi.org/10.1128/JVI.01246-17.
41. Suzuki T, Hasebe A. 2017. A provisional complete genome-based genotyping system for rotavirus species C from terrestrial mammals. J Gen Virol 98:2647–2662. https://doi.org/10.1099/jgv.0.000953.
42. Eren E, Zamuda K, Patton JT. 2016. Modeling of the rotavirus group C capsid predicts a surface topology distinct from other rotavirus species. Virology 487:150–162. https://doi.org/10.1016/j.virol.2015.10.017.
43. Le Pendu J, Nystrom K, Ruvoen-Clouet N. 2014. Host-pathogen coevolution and glycan interactions. Curr Opin Virol 7:88–94. https://doi.org/10.1016/j.coviro.2014.06.001.
44. Ramani S, Hu L, Venkataram Prasad BV, Estes MK. 2016. Diversity in rotavirus-host glycan interactions: a "sweet" spectrum. Cell Mol Gastroenterol Hepatol 2:263–273. https://doi.org/10.1016/j.jcmgh.2016.03.002.
45. Banyai K, Bogdan A, Domonkos G, Kisfali P, Molnar P, Toth A, Melegh B, Martella V, Gentsch JR, Szucs G. 2009. Genetic diversity and zoonotic potential of human rotavirus strains, 2003–2006, Hungary. J Med Virol 81:362–370. https://doi.org/10.1002/jmv.21375.
46. Jonesteller CL, Burnett E, Yen C, Tate JE, Parashar UD. 2017. Effectiveness of rotavirus vaccination: a systematic review of the first decade of global postlicensure data, 2006–2016. Clin Infect Dis 65:840–850. https://doi.org/10.1093/cid/cix369.
47. Sun X, Li D, Peng R, Guo N, Jin M, Zhou Y, Xie G, Pang L, Zhang Q, Qi J, Duan ZJ. 2016. Functional and structural characterization of P[19] rotavirus VP8* interaction with histo-blood group antigens. J Virol 90:9758–9765. https://doi.org/10.1128/JVI.01566-16.
48. Cholleti SR, Agravat S, Morris T, Saltz JH, Song X, Cummings RD, Smith DF. 2012. Automated motif discovery from glycan array data. OMICS 16:497–512.
49. Tamura K, Stecher G, Peterson D, Filipski A, Kumar S. 2013. MEGA6: molecular evolutionary genetics analysis version 6.0. Mol Biol Evol 30:2725–2729. https://doi.org/10.1093/molbev/mst197.
50. Otwinowski Z, Minor W. 1997. Processing of X-ray diffraction data collected in oscillation mode. Methods Enzymol 276:307–326. https://doi.org/10.1016/S0076-6879(97)76066-X.
51. Winn MD, Ballard CC, Cowtan KD, Dodson EJ, Emsley P, Evans PR, Keegan RM, Krissinel EB, Leslie AG, McCoy A, McNicholas SJ, Murshudov GN, Pannu NS, Potterton EA, Powell HR, Read RJ, Vagin A, Wilson KS. 2011. Overview of the CCP4 suite and current developments. Acta Crystallogr D Biol Crystallogr 67:235–242. https://doi.org/10.1107/S0907444910045749.
52. Sheldrick GM. 2010. Experimental phasing with SHELXC/D/E: combining chain tracing with density modification. Acta Crystallogr D Biol Crystallogr 66:479–485. https://doi.org/10.1107/S0907444909038360.
53. McCoy AJ, Grosse-Kunstleve RW, Adams PD, Winn MD, Storoni LC, Read RJ. 2007. Phaser crystallographic software. J Appl Crystallogr 40:658–674. https://doi.org/10.1107/S0021889807021206.
54. Cowtan KD, Zhang KY. 1999. Density modification for macromolecular phase improvement. Prog Biophys Mol Biol 72:245–270. https://doi.org/10.1016/S0079-6107(99)00008-5.
55. Emsley P, Cowtan K. 2004. Coot: model-building tools for molecular graphics. Acta Crystallogr D Biol Crystallogr 60:2126–2132. https://doi.org/10.1107/S0907444904019158.
56. Afonine PV, Grosse-Kunstleve RW, Echols N, Headd JJ, Moriarty NW, Mustyakimov M, Terwilliger TC, Urzhumtsev A, Zwart PH, Adams PD.

2012. Towards automated crystallographic structure refinement with phenix.refine. Acta Crystallogr D Biol Crystallogr 68(Pt 4):352–367. https://doi.org/10.1107/S0907444912001308.
57. Adams PD, Afonine PV, Bunkoczi G, Chen VB, Davis IW, Echols N, Headd JJ, Hung LW, Kapral GJ, Grosse-Kunstleve RW, McCoy AJ, Moriarty NW, Oeffner R, Read RJ, Richardson DC, Richardson JS, Terwilliger TC, Zwart PH. 2010. PHENIX: a comprehensive Python-based system for macromolecular structure solution. Acta Crystallogr D Biol Crystallogr 66:213–221. https://doi.org/10.1107/S0907444909052925.
58. Chen VB, Arendall WB, III, Headd JJ, Keedy DA, Immormino RM, Kapral GJ, Murray LW, Richardson JS, Richardson DC. 2010. MolProbity: all-atom structure validation for macromolecular crystallography. Acta Crystallogr D Biol Crystallogr 66:12–21. https://doi.org/10.1107/S0907444909042073.